

Manipulating the photonic Hall effect with hybrid Mie-exciton resonances

P. Elli Stamatopoulou,^{1,2} Vassilios Yannopoulos,² N. Asger Mortensen,^{1,3} and Christos Tserkezis^{1,*}

¹*Center for Nano Optics, University of Southern Denmark, Campusvej 55, DK-5230 Odense M, Denmark*

²*Department of Physics, National Technical University of Athens, GR-15780 Athens, Greece*

³*Danish Institute for Advanced Study, University of Southern Denmark, Campusvej 55, DK-5230 Odense M, Denmark*

(Dated: August 3, 2020)

We examine the far-field optical response, under plane wave excitation in the presence of a static magnetic field, of core-shell nanoparticles involving a gyroelectric component, either as the inner or the outer layer, through analytic calculations based on appropriately extended Mie theory. We focus on absorption and scattering of light by bismuth-substituted yttrium iron garnet (Bi:YIG) nanospheres and nanoshells, combined with excitonic materials such as organic-molecule aggregates or two-dimensional transition-metal dichalcogenides (TMDs), and discuss the hybrid character of the modes emerging from the coupling of the two constituents. We observe the excitation of strong magneto-optical phenomena and explore, in particular, the response and tunability of a magneto-transverse light current, indicative of the photonic Hall effect. We show how interaction between the Bi:YIG and excitonic layers leads to a pair of narrow bands of highly directional scattering, emerging from the aforementioned hybridization, which can be tuned at will by adjusting the geometrical or optical parameters of the system. Our theoretical study introduces optically anisotropic media as promising templates for strong coupling in nanophotonics, offering a means to combine tunable magnetic and optical properties, with potential implications both in the design of all-dielectric photonic devices but also in novel clinical applications.

I. INTRODUCTION

Scattering and absorption by composite multi-layered nanoparticles (NPs) have long been at the forefront of interest in nanophotonics, with plasmonic structures providing so far the most prominent and fertile template [1–6], aiming to manipulate electromagnetic (EM) fields and generate new, hybrid elements with unique optical properties [7–9]. Plasmons, i.e. collective oscillations of the conduction-band electrons in metals, are known to exhibit a resonant behavior, tunable through the geometrical and optical parameters of the NP, triggering impressive optical phenomena, such as huge enhancement and confinement of light in subwavelength volumes [10]. Nevertheless, high inherent Ohmic losses hinder the widespread use of metals in everyday photonics [11], and focus has recently turned towards high-index dielectrics [12, 13]. In this context, single or composite silicon NPs have been the subject of renewed theoretical and experimental interest, exposing a richness of optical modes, of both electric and magnetic character, generated by oscillating polarization charges and circulating displacement currents inside the particle [13–15]. In contrast to plasmonic assemblies that usually support negligible magnetic modes, dielectrics can be fabricated to combine strong magnetic resonances with low intrinsic losses and enhancement of light comparable to their plasmonic counterparts [16, 17]. Moreover, due to their compatibility with existing technologies in microelectronics and the relative ease of fabrication, all-dielectric nanodevices have been proposed as a promising alternative

to nanoplasmonics with possible applications in biosensing [18], metamaterials [19–21], nanoantennas [22, 23] and slow light [24].

Of particular interest is the case of composite NPs consisting of a dielectric component and an excitonic layer sustained by J -aggregates of organic molecules or two-dimensional (2D) transition-metal dichalcogenides (TMDs), operating at or close to the strong coupling regime. Such architectures offer even broader functionality and flexibility in applications, while also providing crucial new insight into the nature and mechanisms governing light-matter interactions. Recently, silicon- J -aggregate heterostructures have been explored, from both theoretical and experimental aspects, as an alternative to plasmon-exciton hybrids termed plexcitons [7, 25], revealing the formation of hybrid modes of photonic-excitonic character, termed, in an equivalent manner, Mie-excitons [15, 26–29]. In particular, since their emergence in literature, it has been envisaged that the complex, magnetic nature of their modes, would eventually allow to externally manipulate them with static magnetic fields [26] in analogy with active magnetoplasmonics [30], a feature that has not, however, been explored as yet.

At the same time, composite magnetic NPs with core-shell morphology — usually a magnetic core coated with a biocompatible organic dye — are proposed as suitable building blocks for novel clinical applications in nanomedicine, for a diversity of purposes including imaging, drug delivery and photothermal therapy [31–33]. A key advantage of magnetic NPs is their ability to respond to multiple external stimuli (light, magnetic field, temperature, etc) in a non-invasive manner, i.e. without perturbing the biological system. However, the coexistence of light and magnetism in a system characterized by its ability to respond to both gives rise to opti-

*Electronic address: ct@mci.sdu.dk

cal anisotropy, and thus to magneto-optical phenomena, a thorough study of which is required when considering medical applications. The formulation of Mie scattering by optically anisotropic spheres has already been analytically developed [34] and explicitly performed for plasmon-coated Bi:YIG and magnetite particles of various geometries, exposing a prominent plasmon-driven photonic Hall effect and strong magnetochirality [35–38]. In analogy to the classical Hall effect, in its photonic counterpart an incident EM wave propagating through a gyroelectric medium along a direction perpendicular to the applied magnetic field is deflected transversely to both propagation and the magnetic field direction. Although being essential for understanding the underlying physics and for the design of all-dielectric devices, a thorough investigation of the photonic Hall effect in non-plasmonic core-shell assemblies is still missing.

Here, we analyze the photonic Hall effect in composite nanospheres, consisting of a gyroelectric and an excitonic layer. We show that, although not strictly operating in the strong-coupling regime, the interaction of Mie resonances with excitonic modes leads to a hybridization manifested through the splitting of the observed magneto-optic response into two narrow bands, thus allowing to tailor the photonic Hall effect with precision. The remaining paper is structured as follows. In Sec. II we summarize Mie theory for scattering and absorption by coated gyroelectric NPs and nanoshells, and present the scattering cross section formula for the Hall photon current. In Sec. III we present our theoretical results regarding two specific examples, i.e., a Bi:YIG nanosphere with an excitonic coating, and an excitonic core coated with a Bi:YIG nanoshell. Our main findings are summarized in the last section of the article.

II. THEORETICAL METHOD

Let us assume a time-harmonic, monochromatic plane EM wave of angular frequency ω , incident on a gyroelectric sphere of radius R embedded in an infinite homogeneous host medium that is characterized by scalar permittivity and permeability ϵ_2 and μ_2 , in the presence of a static magnetic field. The presence of the magnetic field induces a Lorentz force, which needs to be added in the equations of motion of electrons in the sphere, leading to an anisotropic permittivity tensor [39]. If the orientation of the magnetic field is along the z axis, the permittivity is given by

$$\epsilon_1 = \epsilon_z \begin{pmatrix} \epsilon_r & -i\epsilon_\kappa & 0 \\ i\epsilon_\kappa & \epsilon_r & 0 \\ 0 & 0 & 1 \end{pmatrix} \quad (1)$$

while the permeability μ_1 is scalar, practically equal to unity in the optical regime [40]. The tensor components are in general complex functions of frequency, taking dispersion and dissipative losses into account while naturally being causal and fulfilling Kramers–Kronig relations.

The fields inside and outside the sphere can be expressed in the basis of vector spherical harmonics. Given the electric field component \mathbf{E}_0 of the incoming plane wave, the incident electric field can be written as

$$\mathbf{E}_{\text{inc}} = \mathbf{E}_0 e^{i\mathbf{k}\cdot\mathbf{r}} = \sum_{Plm} a_{Plm}^0 \mathbf{F}_{Plm}, \quad (2)$$

where $P = H, E$ refers to the polarization, l and m are the angular momentum indices, $\mathbf{F}_{Hlm}, \mathbf{F}_{Elm}$ are the transverse magnetic and electric wave functions respectively, explicitly given later on, $\mathbf{a}^0 = [a_{Hlm} \ a_{Elm}]^T$ with $l \in [1, \infty)$ and $m \in [-l, l]$ is the amplitude of the incident wave (see Appendix) and $\mathbf{a}^+ = \mathbf{T} \cdot \mathbf{a}^0$ the amplitude of the scattered spherical wave, where \mathbf{T} is the scattering matrix. The infinite expansion series describing the fields inside and outside the particle can be truncated in practice at a certain value l_{max} and in this case the amplitudes are $(n_d \times 1)$ column vectors, where $n_d = l_{\text{max}}(l_{\text{max}} + 2)$. It can be shown that \mathbf{T} takes the form [41]

$$\mathbf{T} = \mathbf{Z} \cdot (\mathbf{U} + \mathbf{\Lambda} \cdot \mathbf{Z})^{-1} \quad (3)$$

with

$$\mathbf{Z} = (\mathbf{\Lambda} - \mathbf{\Lambda}')^{-1} \cdot (\mathbf{V} - \mathbf{U}), \quad (4)$$

where the matrices $\mathbf{\Lambda}, \mathbf{\Lambda}', \mathbf{V}, \mathbf{U}$ are provided in the Appendix.

Having calculated the scattering matrix \mathbf{T} , the extinction, scattering and absorption cross sections, normalized to the geometric cross section πR^2 , are obtained by [42]

$$\sigma_{\text{sc}} = \frac{1}{(k_2 R)^2 \pi |E_0|^2} \sum_{Plm} |a_{Plm}^+|^2 \quad (5a)$$

$$\sigma_{\text{abs}} = -\frac{1}{(k_2 R)^2 \pi |E_0|^2} \left\{ \sum_{Plm} |a_{Plm}^+|^2 + \text{Re} \left(\sum_{P'l'm'} a_{P'l'm'}^0 \dagger \cdot \sum_{Plm} a_{Plm}^+ \right) \right\} \quad (5b)$$

$$\sigma_{\text{ext}} = \sigma_{\text{sc}} + \sigma_{\text{abs}} = -\frac{1}{(k_2 R)^2 \pi |E_0|^2} \text{Re} \left(\sum_{P'l'm'} a_{P'l'm'}^0 \dagger \cdot \sum_{Plm} a_{Plm}^+ \right). \quad (5c)$$

We now consider the above gyroelectric sphere of radius R_1 , coated with a concentric spherical shell of radius R_2 and optical parameters ϵ_2 and μ_2 — index 3 now refers to parameters of the host medium, as shown in the schematics of Fig. 1. Boundary conditions at the outer surface S_2 of the composite sphere require continuity of the tangential components of the electric and the magnetic field, yielding

$$\mathbf{a}^+ = \tilde{\mathbf{\Lambda}} \mathbf{a}^0 + \tilde{\mathbf{U}} \mathbf{a}^0 \quad (6a)$$

$$\mathbf{a}^+ = \tilde{\mathbf{\Lambda}}' \mathbf{a}^0 + \tilde{\mathbf{V}} \mathbf{a}^0, \quad (6b)$$

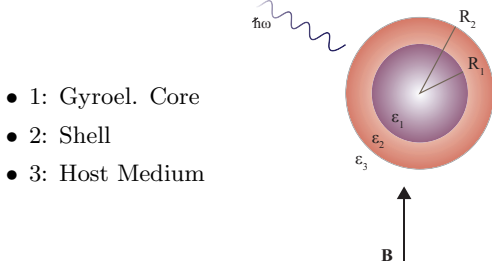


FIG. 1: A nanosphere consisting of a gyroelectric core and an isotropic shell of inner radius R_1 and outer R_2 illuminated by a plane EM wave in the presence of an external static magnetic field \mathbf{B} .

where

$$\tilde{\mathbf{U}} = \mathbf{U}_A \cdot \mathbf{T} + \mathbf{U}_B \quad (7a)$$

$$\tilde{\mathbf{V}} = \mathbf{V}_A \cdot \mathbf{T} + \mathbf{V}_B \quad (7b)$$

(see Appendix for matrices $\tilde{\mathbf{A}}, \tilde{\mathbf{A}}', \mathbf{U}_A, \mathbf{U}_B, \mathbf{V}_A, \mathbf{V}_B$).

Equations (6) lead to the following expression for the scattering matrix of the core-shell system:

$$\tilde{\mathbf{T}} = \tilde{\mathbf{Z}} \cdot \tilde{\mathbf{R}} \quad (8)$$

with

$$\tilde{\mathbf{Z}} = (\tilde{\mathbf{U}}^{-1} - \tilde{\mathbf{V}}^{-1})^{-1} \quad (9)$$

$$\tilde{\mathbf{R}} = (\tilde{\mathbf{U}}^{-1}\tilde{\mathbf{A}} - \tilde{\mathbf{V}}^{-1}\tilde{\mathbf{A}}'). \quad (10)$$

We will now derive the scattering matrix of the inverse core-shell configuration, that is, a gyroelectric shell with a homogeneous medium both inside the cavity and as the host environment, as shown in Fig. 2. The wave equation of the electric displacement vector \mathbf{D}_2 inside the gyroelectric shell can be obtained by substituting Eq. (1) into the source-free Maxwell equations, that is

$$\nabla \times \nabla \times [\epsilon_z \epsilon_g^{-1} \mathbf{D}(\mathbf{r})] - k_2^2 \mathbf{D}(\mathbf{r}) = 0, \quad (11)$$

with $k_2^2 = \omega^2 \epsilon_z \epsilon_0 \mu_2 \mu_0$ being the wavenumber in medium 2.

Similarly to the procedure followed in [41], one can show now that the fields in the second layer are:

$$\begin{aligned} \mathbf{E}(\mathbf{r}) = & \sum_j b_j \left\{ \frac{k_j^2}{k_2^2} \bar{w}_{00;j} \mathbf{J}_{L00} + \sum_{lm} \left[\frac{k_j^2}{k_2^2} \bar{w}_{lm;j} \mathbf{J}_{Llm} \right. \right. \\ & \left. \left. + a_{Hlm;j} \mathbf{J}_{Hlm} + a_{Elm;j} \mathbf{J}_{Elm} \right] \right\} \\ & + \sum_j c_j \left\{ \frac{k_j^2}{k_2^2} \bar{w}_{00;j} \mathbf{H}_{L00} + \sum_{lm} \left[\frac{k_j^2}{k_2^2} \bar{w}_{lm;j} \mathbf{H}_{Llm} \right. \right. \\ & \left. \left. + a_{Hlm;j} \mathbf{H}_{Hlm} + a_{Elm;j} \mathbf{H}_{Elm} \right] \right\} \end{aligned} \quad (12)$$

and

$$\mathbf{H}(\mathbf{r}) = \sum_j b_j \frac{k_j^2}{\omega \mu_0 \mu_2} \sum_{lm} \left[a_{Elm;j} \mathbf{J}_{Hlm} - a_{Hlm;j} \mathbf{J}_{Elm} \right] \quad (13)$$

$$+ \sum_j c_j \frac{k_j^2}{\omega \mu_0 \mu_2} \sum_{lm} \left[a_{Elm;j} \mathbf{H}_{Hlm} - a_{Hlm;j} \mathbf{H}_{Elm} \right]$$

with

$$\mathbf{F}_{Hlm}(\mathbf{r}) = f_l(kr) \mathbf{X}_{lm}(\hat{\mathbf{r}}) \quad (14)$$

$$\mathbf{F}_{Elm}(\mathbf{r}) = \frac{i}{k} \nabla \times f_l(kr) \mathbf{X}_{lm}(\hat{\mathbf{r}}) \quad (15)$$

$$\mathbf{F}_{Llm}(\mathbf{r}) = \frac{i}{k} \nabla [f_l(kr) Y_{lm}(\hat{\mathbf{r}})] \quad (16)$$

representing transverse magnetic, transverse electric and longitudinal wave functions respectively, while $f_l = j_l, h_l$ corresponds to either the spherical Bessel or Hankel function, $\mathbf{X}_{lm}(\hat{\mathbf{r}})$ are the vector spherical harmonics, and Y_{lm} are the ordinary spherical harmonics [43].

Boundary conditions at the inner and outer surface determine the expression for the scattering matrix \mathbf{T} :

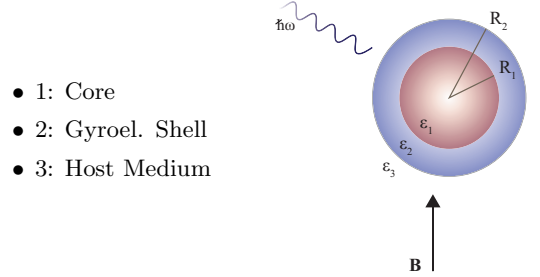


FIG. 2: A nanosphere of excitonic-gyroelectric core-shell configuration, of inner radius R_1 and outer R_2 , illuminated by a plane EM wave in the presence of an external static magnetic field \mathbf{B} .

$$\mathbf{Z} = (\mathcal{L} - \mathcal{L}')^{-1} \cdot (\mathcal{V} - \mathcal{U}) \quad (17)$$

$$\mathbf{R} = (\mathcal{U} + \mathcal{L} \cdot \mathbf{Z})^{-1} \quad (18)$$

$$\mathbf{T} = \mathbf{Z} \cdot \mathbf{R}, \quad (19)$$

where

$$\mathcal{U} = \mathbf{U}_1^{\mathbf{S}2} \cdot \mathbf{M} + \mathbf{U}_2^{\mathbf{S}2} \quad (20a)$$

$$\mathcal{V} = \mathbf{V}_1^{\mathbf{S}2} \cdot \mathbf{M} + \mathbf{V}_2^{\mathbf{S}2} \quad (20b)$$

$$\mathbf{M} = \left(\mathbf{U}_1^{\mathbf{S}1} - \mathbf{V}_1^{\mathbf{S}1} \right)^{-1} \cdot \left(\mathbf{V}_2^{\mathbf{S}1} - \mathbf{U}_2^{\mathbf{S}1} \right). \quad (20c)$$

The matrices entering the above formulas can be found in the Appendix.

An incident EM wave with linear polarization causes displacement of charge carriers along the direction of the

electric field oscillation. The Lorentz force that acts on this movement in the presence of the magnetic field is perpendicular to both the magnetic field and the electric field polarization ($\mathbf{F}_L \propto \mathbf{v} \times \mathbf{B}$), where \mathbf{v} is the velocity of the carriers. So in our case, if a y -polarized wave propagates along the x axis and the magnetic field is along z axis, the Lorentz force induces a polarization of charges along the $\hat{\mathbf{y}} \times \hat{\mathbf{z}} = \hat{\mathbf{x}}$ axis, corresponding to the photonic Hall effect. As a result, there is a component of light scattered along the $\hat{\mathbf{y}}$ direction. It has been shown by Varytis *et al.* [35] that the scattering cross section of this transverse component σ_{Hall} along the $\hat{\mathbf{y}}$ axis is given by the following exact analytic expression:

$$\sigma_{\text{Hall}} = \frac{1}{\pi |\mathbf{E}_0|^2} \frac{1}{(k_2 R)^2} \text{Re} \left\{ \sum_{lm} \left[\frac{a_l^{-m}}{l(l+1)} (a_{Hlm}^+ a_{Elm-1}^{+*} - a_{Elm}^+ a_{Hlm-1}^{+*}) - \xi_{l-1}^{m-1} (a_{Hlm}^+ a_{Hl-1m-1}^{+*} + a_{Elm}^+ a_{El-1m-1}^{+*}) - \xi_{l-1}^{-m-1} (a_{Hlm}^+ a_{Hl-1m+1}^{+*} + a_{Elm}^+ a_{El-1m+1}^{+*}) \right] \right\}, \quad (21)$$

where the amplitudes a_{Plm}^+ compose the column vector of the scattered wave, with

$$a_l^m = \frac{1}{2} \sqrt{(l-m)(l+m+1)} \quad (22)$$

and

$$\xi_l^m = \frac{1}{2(l+1)} \sqrt{\frac{l(l+2)(l+m+1)(l+m+2)}{(2l+1)(2l+3)}}. \quad (23)$$

III. RESULTS AND DISCUSSION

To design a Mie-excitonic system with strong and tunable photonic Hall effect, we will perform an analytic study of composite core-shell NPs consisting of a gyroelectric and an excitonic layer embedded in air. We assume, to begin with, a plane wave propagating along the x axis, incident on a Bi:YIG sphere of radius $R_1 = 100$ nm, while subjected to a static magnetic field oriented along the z axis. Bi:YIG is chosen as a typical gyroelectric high-index dielectric material, characterized by the experimental optical parameters of [44] (measured at saturation) reproduced in Figs. 3(a)-(b).

As shown in Fig. 3(c), the extinction and scattering cross sections of this particle, in the visible part of the spectrum, are characterized by a pronounced resonance at 2.24 eV, attributed to the magnetic dipole Mie mode, over a wide but weak electric dipolar background [for the decomposition of the extinction spectrum into its multipolar contributions see Fig. 3(d)], whereas higher order contributions are almost negligible. This behavior is

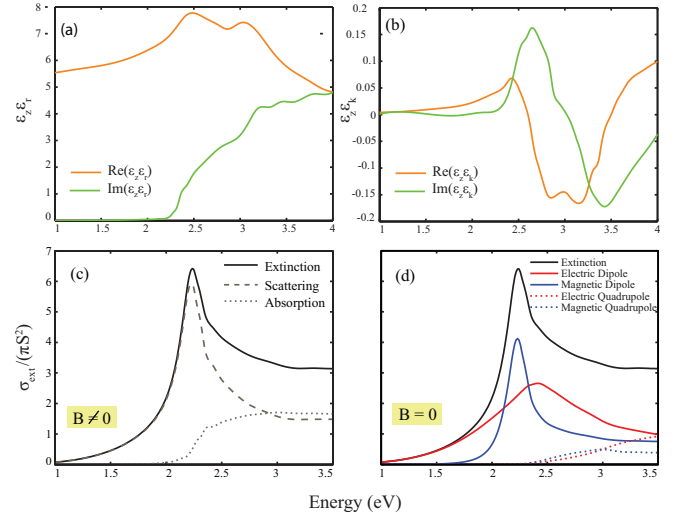


FIG. 3: The real (orange line) and imaginary (green line) part of the (a) diagonal and (b) non-diagonal elements of the permittivity tensor [Eq. (1)] of Bi:YIG [44]. (c) Extinction (black solid line), scattering (grey dashed line) and absorption (grey dotted line) cross sections normalized to the geometric cross section of a Bi:YIG nanosphere of radius $R_1 = 100$ nm subjected to a static magnetic field embedded in air. (d) Magnetic (blue) and electric (red) dipolar (solid lines) and quadrupolar (dotted lines) contributions to the extinction cross section (black solid line) for the particle of (c) in the absence of the magnetic field.

quite reminiscent of the response of Si NPs [14]; what it offers additionally, however, is the non-negligible response to an external magnetic field, contrary to what one might at first anticipate from Figs. 3(c) and (d). While comparison between the extinction spectra in the presence and absence of the static magnetic field shows that the position and width of the magnetic dipolar resonance is practically not affected, one should not forget that, first, Bi:YIG reaches saturation at relatively weak magnetic fields [45] and, secondly, any magneto-optic properties, including the photonic Hall effect, are completely eliminated when the field is turned off. The absorption spectrum does not exhibit a Lorentzian-like peak, but a plateau instead, as one could expect from the permittivity data of Figs. 3(a) and (b). The large positive value in the imaginary part of the diagonal elements of the permittivity tensor for energies larger than 2.5 eV reveals that this plateau appears most probably due to interband transitions.

The magneto-optical properties arising in gyrotropic media owe their existence to the non-diagonal components of the permittivity tensor and vanish above the Curie temperature (here $T_C \approx 590$ K [46]). For the Bi:YIG sphere the non-diagonal elements are large enough to produce magneto-optical phenomena [Fig. 3(b)]. In the present work we shall only be concerned with the photonic Hall effect, but similar conclusions should, in principle, apply to any other mani-

festations of magneto-optics, such as the Faraday, Kerr, or magnetochiral effects [38, 47, 48]. As displayed in Fig. 4(b) with the black dashed line, a strong component of magneto-transverse scattered light arises at 2.21 eV, close to the magnetic dipolar mode, also exhibiting a resonant behavior.

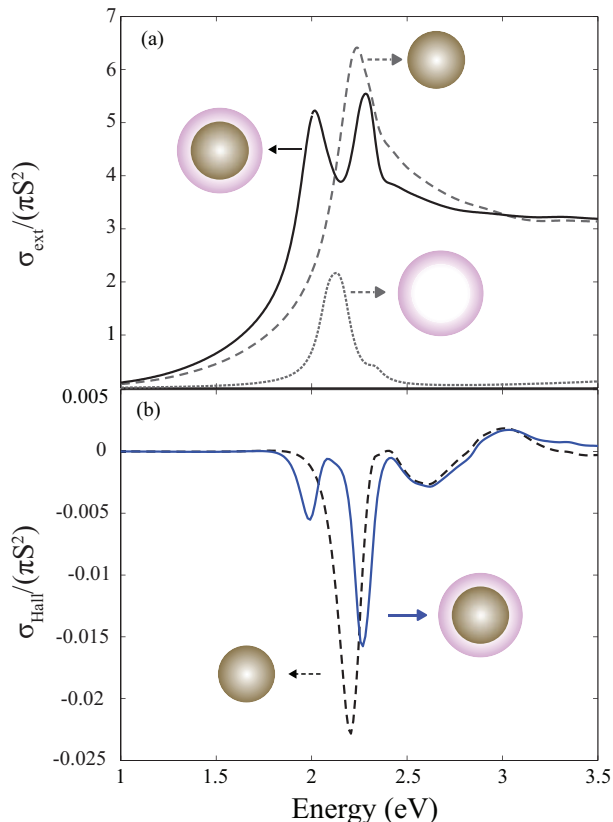


FIG. 4: (a) Extinction cross section of a Bi:YIG NP of radius $R_1 = 100$ nm (grey dashed line), an excitonic shell of inner radius $R_1 = 100$ nm and outer $R_2 = 110$ nm (grey dotted line), and a core-shell NP consisting of the Bi:YIG core and the excitonic shell. (b) Cross section of the magneto-transverse scattered light of the Bi:YIG NP (black dashed line) and the exciton-coated Bi:YIG core (blue solid line), as depicted in the schematics. In all panels air is the host medium.

Let us now consider a composite particle consisting of a spherical Bi:YIG core and a concentric excitonic shell of thickness $R_2 - R_1 = w = 10$ nm. Such a design can be synthesized relatively easily in the laboratory and constitutes a flexible platform for engineering the hybrid Mie-excitons [26]. For the excitonic material we use the following generic dielectric function:

$$\epsilon_{\text{exc}}(\omega) = \epsilon_{\infty} - \frac{f\omega_{\text{exc}}^2}{\omega^2 - \omega_{\text{exc}}^2 - i\omega\gamma_{\text{exc}}}, \quad (24)$$

where ω_{exc} is the excitonic transition frequency, γ_{exc} the corresponding damping rate, f the oscillator strength

and ϵ_{∞} the background permittivity. For our calculation we choose $\hbar\omega_{\text{exc}} = 2.12$ eV, $\hbar\gamma_{\text{exc}} = 0.1$ eV, $f = 0.65$ and $\epsilon_{\infty} = 3$, values that do not correspond to a particular dye, but can be considered realistic. The parameters of the excitonic layer have been chosen so that its resonance frequency lies close to the dipolar magnetic Mie mode of the core. Fig. 4(a) illustrates the extinction spectra of the two constituents individually (grey lines), together with the spectrum resulting from the coupling of the two layers (black solid line). The interaction of the two components leads to the hybridization of their modes, which manifests in the spectra by the emergence of two resonances, separated by an anticrossing of width $\hbar\Omega = 0.27$ eV. It is perhaps tempting to claim that the system has entered the strong-coupling regime [49], but application of the usual linewidth criterion, which requires that the split squared must be larger than half the sum of the uncoupled linewidths squared, shows that this is not the case yet ($0.27 \text{ eV} < \sqrt{(0.37^2 + 0.17^2)}/2 \text{ eV} = 0.29 \text{ eV}$). The situation is thus closer to what has been termed induced transparency [50]. The inability to satisfy the strong coupling criteria is due to the extremely broad resonance of Bi:YIG, which is not fully compatible with the linewidths of usual organic dyes.

As a result of the addition of the excitonic layer, the pronounced peak of the Hall photon current splits in two peaks of slightly lower intensity [blue line in Fig. 4(b)], following the double peak behavior of the extinction spectrum. The split indicates a hybrid mode of mixed light-matter nature emerging from two coupled modes with an energy difference of 0.28 eV coupled in analogy to the formation of bonding and antibonding electron states in molecules.

In what follows, we invert the arrangement of the two layers and study the photonic Hall effect of an excitonic core-gyroelectric shell configuration of inner and outer radius $R_1 = 60$ nm and $R_2 = 110$ nm, respectively. It should be noted here that such architectures, challenging as they might be in both fabrication and application in nanobiotechnology, are beneficial in the theoretical search for strongly-coupled systems, and they usually provide a clearer physical picture which facilitates understanding of the origin of each spectral feature [26].

The excitonic material is described by the dielectric function of Eq. (24) with $\hbar\omega_{\text{exc}} = 2.05$ eV, $\hbar\gamma_{\text{exc}} = 0.04$ eV, $f = 0.3$ and $\epsilon_{\infty} = 3$. When the excitonic resonance is disregarded, i.e. $f = 0$ in the dielectric function of Eq. (24), the far-field optical response of the Bi:YIG shell [grey dashed line in Fig. 5(a)] does not differ significantly from that of the Bi:YIG sphere of Fig. 3(b), exhibiting a well-defined magnetic Mie resonance at 2.18 eV. As depicted in Fig. 5(a), the excitonic core and the gyroelectric shell have been constructed so that the resulting resonances appear at similar energies, leading once again to the double-peak spectrum of the coupled system. Once again the Hall photon current of the gyroelectric nanoshell exhibits resonant spectral features about the Mie mode, as expected. However,

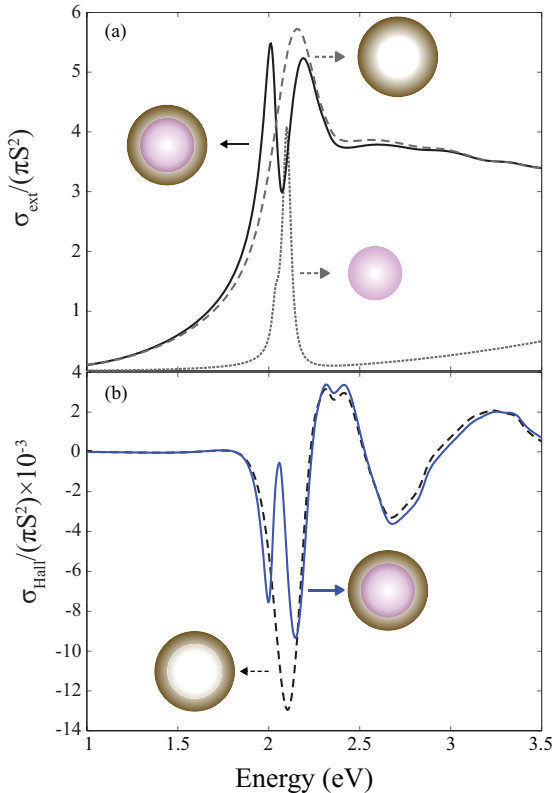


FIG. 5: (a) Extinction cross section of an excitonic NP of radius $R_1 = 60$ nm (grey dotted line), a core-shell NP consisting of a Bi:YIG shell and the excitonic NP of inner radius $R_1 = 60$ nm and outer $R_2 = 110$ nm, disregarding the excitonic resonance (grey dotted line) and same configuration as taking into account the excitonic transition. (b) Cross section of the magneto-transverse scattered light of the Bi:YIG shell (black dashed line) and the Bi:YIG shell – excitonic core NP (blue solid line), as depicted in the schematics illustrations. In all panels air is the host medium.

Fig. 5(b) shows that it is weaker in comparison to the case of the solid gyroelectric nanosphere. Taking the excitonic resonance into account [$f = 0.3$ in Eq. (24)] has similar effect on the σ_{Hall} spectrum as before; namely the single broad resonance of Bi:YIG at 2.10 eV has been split into two narrower ones, which can be important in applications requiring highly directional scattering in a narrow frequency window. In comparison to the inverse configuration of Fig. 4(b), this arrangement exhibits two narrow peaks comparable to each other in both width and magnitude.

Tunability of these modes is a major advantage. An increase or a decrease in the radius of the composite particle results in redshifting or blueshifting of the Mie modes respectively. It is therefore straightforward that the maximum of the magneto-transverse scattered light shifts accordingly. A rather interesting aspect of the flexibility of such assemblies, especially in strong light–matter interaction studies, is the fact that wider splits of the

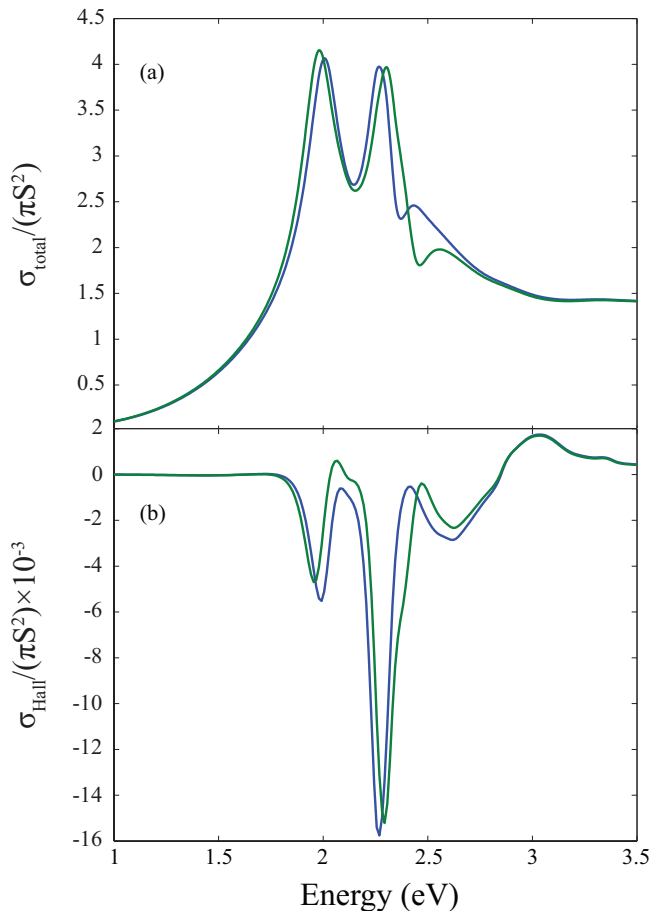


FIG. 6: (a) Total scattering cross section of a core-shell NP consisting of a Bi:YIG core and an excitonic shell of inner radius $R_1 = 100$ nm and outer $R_2 = 110$ nm, with i) oscillator strength $f = 0.65$ (blue line) and ii) $f = 0.95$ (green line) in (24). (b) Cross section of the magneto-transverse scattered light of configurations i) (blue line) and ii) (green line).

hybrid modes can be achieved by increasing the oscillator strength of the excitonic dielectric function. Already the double-peak spectrum of Figs. 4 and 5 indicates strongly coupled regimes and controllability of the coupling strength is possible, as shown in Fig. 6. In particular, in the case of the gyroelectric core–excitonic shell NP, increasing the oscillatory strength to $f = 0.95$ leads to slightly lower total scattering cross section as well as to a wider split up to 0.33 eV. The same behavior is reproduced by the Hall photon current in Fig. 6(b), forming a splitting of 0.34 eV, which is 0.06 eV larger compared to that of Fig. 4(b). Alternative routes for higher tunability can be achieved by considering more sophisticated architectures of more layers or of various geometries. Magneto-optical properties of complex plasmon-gyroelectric structures, such as clusters and helices, have already been studied [37, 38], but a non-plasmonic approach is still missing. A tri-layered system, comprising all three kinds of components (plasmonic, excitonic and

magneto-optic) could be a promising route to further enhance the observed effects, although analyzing the hybridization of three different modes in that case might not be straightforward.

IV. CONCLUSIONS

In summary, an analytic method, based on an extended Mie scattering theory, to calculate the Hall photon current for core-shell NPs comprising a gyroelectric layer is provided, based on Mie theory. Previous work on the photonic Hall effect has been limited to single gyrotropic spheres and metal-coated gyrotropic nanospheres characterized by plasmonic-driven magneto-optic phenomena. Here, strong magnetically induced optical phenomena in dielectrics coupled to excitons are reported by studying the photonic Hall effect in two-layered Bi:YIG–excitonic nanospheres. We show that these composite particles exhibit a rich optical response and a prominent photon Hall current, opening new opportunities for multifunctional dielectric-based photonic platforms, tunable by their geometrical and optical parameters, capable to respond to various external stimuli. Rigorous investigation of the Hall activity is crucial for clinical applications, especially for techniques in which directionality is a key issue.

Acknowledgments

We thank P. Varytis for sharing the interpolated data for the optical parameters of Bi:YIG and C. Wolff for discussions. P. E. S. acknowledges support from an Erasmus+ Scholarship. N. A. M. is a VILLUM Investigator supported by VILLUM FONDEN (grant No. 16498) and Independent Research Funding Denmark (grant no. 7026-00117B). The Center for Nano Optics is financially supported by the University of Southern Denmark (SDU 2020 funding).

Appendix

The amplitudes of the incident field are determined by expanding $\exp(\mathbf{i}\mathbf{k}\cdot\mathbf{r})$ in spherical harmonics [43]:

$$a_{Elm}^0 = \frac{4\pi i^l (-1)^{m+1}}{\sqrt{l(l+1)}} \times \left[\{a_l^m Y_{l-(m+1)}(\hat{\mathbf{k}}) + a_l^{-m} Y_{l-(m-1)}(\hat{\mathbf{k}})\} (\mathbf{k} \times \mathbf{E}_0)_x + i^l \{a_l^m Y_{l-(m+1)}(\hat{\mathbf{k}}) - a_l^{-m} Y_{l-(m-1)}(\hat{\mathbf{k}})\} (\mathbf{k} \times \mathbf{E}_0)_y - m Y_{l-m}(\hat{\mathbf{k}}) (\mathbf{k} \times \mathbf{E}_0)_z \right] \quad (25)$$

and

$$a_{Hlm}^0 = \frac{4\pi i^l (-1)^{m+1}}{\sqrt{l(l+1)}} \times \left[\{a_l^m Y_{l-(m+1)}(\hat{\mathbf{k}}) + a_l^{-m} Y_{l-(m-1)}(\hat{\mathbf{k}})\} E_{0x} + i^l \{a_l^m Y_{l-(m+1)}(\hat{\mathbf{k}}) - a_l^{-m} Y_{l-(m-1)}(\hat{\mathbf{k}})\} E_{0y} - m Y_{l-m}(\hat{\mathbf{k}}) E_{0z} \right], \quad (26)$$

where a_l^m is given by Eq. (22).

Matrices \mathbf{A} , \mathbf{A}' , \mathbf{V} , \mathbf{U} used in the calculation of the scattering matrix \mathbf{T} of a single gyroelectric sphere are given by

$$\Lambda_{Plm;P'l'm'} = -\frac{H_{l2}}{J_{l2}} \delta_{ll'} \delta_{mm'} \delta_{PP'} \quad (27a)$$

$$\Lambda'_{Plm;P'l'm'} = -\frac{H'_{l2}}{J'_{l2}} \delta_{ll'} \delta_{mm'} \delta_{PP'} \quad (27b)$$

$$U_{Hlm;j} = \frac{J_{l;j}}{J_{l2}} a_{Hlm;j}^0 \quad (27c)$$

$$U_{Elm;j} = \frac{\mu_2 k_j}{\mu_1 k_2} \frac{J_{l;j}}{J_{l2}} a_{Elm;j}^0 \quad (27d)$$

$$V_{Hlm;j} = \frac{\mu_2}{\mu_1} \frac{J'_{l;j}}{J'_{l2}} a_{Hlm;j} \quad (27e)$$

$$V_{Elm;j} = \frac{k_2}{k_j} \frac{J'_{l;j}}{J'_{l2}} a_{Elm;j} - \frac{\sqrt{l(l+1)} k_j k_2}{k_1^2} \frac{J_{l;j}}{J'_{l2}} \bar{w}_{lm;j}. \quad (27f)$$

In the above formulas we have used the notation $J_{li} = j_l(k_i R)$, $H_{li} = h_l(k_i R)$, $J'_{li} = \frac{\partial}{\partial r} [j_l(k_i r)]|_{r=R}$ and $H'_{li} = \frac{\partial}{\partial r} [h_l(k_i r)]|_{r=R}$, where j_l and h_l are the spherical Bessel and Hankel functions respectively. The wavenumbers k_j and amplitudes $a_{Plm;j}$ are obtained from the solution of the eigenvalue problem

$$\sum_{P'l'm'} A_{Plm;P'l'm'} a_{Plm;j} = \frac{k_g^2}{k^2} a_{Plm;j} \quad (28)$$

where the subscript $j = 1, 2, \dots, 2n_d$ enumerates the eigenvalues and eigenvectors of matrix \mathbf{A} and b_j is a scalar coefficient. Explicit expressions for the matrix elements of \mathbf{A} and for $w_{lm;j}$ entering the formulas are provided in [41].

For the scattering matrix of the coated gyroelectric

sphere, the following matrices enter into the calculation:

$$\tilde{\Lambda}_{Plm;P'l'm'} = -\frac{J_{l3}}{H_{l3}} \delta_{ll'} \delta_{mm'} \delta_{PP'} \quad (29a)$$

$$\tilde{\Lambda}'_{Plm;P'l'm'} = -\frac{J'_{l3}}{H'_{l3}} \delta_{ll'} \delta_{mm'} \delta_{PP'} \quad (29b)$$

$$U_{A,Hlm} = \frac{H_{l2}}{H_{l3}} \delta_{ll'} \delta_{mm'} \quad (29c)$$

$$U_{A,Elm} = \sqrt{\frac{\mu_3 \epsilon_2}{\mu_2 \epsilon_3}} \frac{H_{l2}}{H_{l3}} \delta_{ll'} \delta_{mm'} \quad (29d)$$

$$U_{B,Hlm} = \frac{J_{l2}}{H_{l3}} \delta_{ll'} \delta_{mm'} \quad (29e)$$

$$U_{B,Elm} = \sqrt{\frac{\mu_3 \epsilon_2}{\mu_2 \epsilon_3}} \frac{J_{l2}}{H_{l3}} \delta_{ll'} \delta_{mm'} \quad (29f)$$

$$V_{A,Hlm} = \frac{\mu_3 H'_{l2}}{\mu_2 H'_{l3}} \delta_{ll'} \delta_{mm'} \quad (29g)$$

$$V_{A,Elm} = \frac{k_3 H'_{l2}}{k_2 H'_{l3}} \delta_{ll'} \delta_{mm'} \quad (29h)$$

$$V_{B,Hlm} = \frac{\mu_3 J'_{l2}}{\mu_2 H'_{l3}} \delta_{ll'} \delta_{mm'} \quad (29i)$$

$$V_{B,Elm} = \frac{k_3 J'_{l2}}{k_2 H'_{l3}} \delta_{ll'} \delta_{mm'}. \quad (29j)$$

For the scattering matrix of the inverse configuration the matrices used are calculated by

$$U_{1,Hlm}^{S_1} = \frac{J_{l;j}}{J_{l1}} a_{Hlm;j} \delta_{ll'} \delta_{mm'} \quad (30a)$$

$$U_{1,Elm}^{S_1} = \frac{k_j \mu_1 J_{l;j}}{k_1 \mu_2 J_{l1}} a_{Elm;j} \delta_{ll'} \delta_{mm'} \quad (30b)$$

$$U_{2,Hlm}^{S_1} = \frac{H_{l;j}}{J_{l1}} a_{Hlm;j} \delta_{ll'} \delta_{mm'} \quad (30c)$$

$$U_{2,Elm}^{S_1} = \frac{k_j \mu_1 H_{l;j}}{k_1 \mu_2 J_{l1}} a_{Elm;j} \delta_{ll'} \delta_{mm'} \quad (30d)$$

$$V_{1,Hlm}^{S_1} = \frac{\mu_1 J'_{l;j}}{\mu_2 J'_{l1}} a_{Hlm;j} \quad (30e)$$

$$V_{1,Elm}^{S_1} = \frac{k_1 J'_{l;j}}{k_j J'_{l1}} a_{Elm;j} - \frac{k_j k_1}{k_2^2} \sqrt{l(l+1)} \bar{w}_{lm;j} \frac{J_{l;j}}{J'_{l1}} \quad (30f)$$

$$V_{2,Hlm}^{S_1} = \frac{\mu_1 H'_{l;j}}{\mu_2 J'_{l1}} a_{Hlm;j} \quad (30g)$$

$$V_{2,Elm}^{S_1} = \frac{k_1 H'_{l;j}}{k_j J'_{l1}} a_{Elm;j} - \frac{k_j k_1}{k_2^2} \sqrt{l(l+1)} \bar{w}_{lm;j} \frac{H_{l;j}}{J'_{l1}}. \quad (30h)$$

$$\mathcal{L}_{Plm;P'l'm'} = -\frac{H_{l3}}{J_{l3}} \delta_{ll'} \delta_{mm'} \delta_{PP'} \quad (30i)$$

$$\mathcal{L}'_{Plm;P'l'm'} = -\frac{H'_{l3}}{J'_{l3}} \delta_{ll'} \delta_{mm'} \delta_{PP'} \quad (30j)$$

$$U_{1,Hlm}^{S_2} = \frac{J_{l;j}}{J_{l3}} a_{Hlm;j} \delta_{ll'} \delta_{mm'} \quad (30k)$$

$$U_{1,Elm}^{S_2} = \frac{k_j \mu_3 J_{l;j}}{k_3 \mu_2 J_{l3}} a_{Elm;j} \delta_{ll'} \delta_{mm'} \quad (30l)$$

$$U_{2,Hlm}^{S_2} = \frac{H_{l;j}}{J_{l3}} a_{Hlm;j} \delta_{ll'} \delta_{mm'} \quad (30m)$$

$$U_{2,Elm}^{S_2} = \frac{k_j \mu_3 H_{l;j}}{k_3 \mu_2 J_{l3}} a_{Elm;j} \delta_{ll'} \delta_{mm'} \quad (30n)$$

$$V_{1,Hlm}^{S_2} = \frac{\mu_3 J'_{l;j}}{\mu_2 J'_{l3}} a_{Hlm;j} \quad (30o)$$

$$V_{1,Elm}^{S_2} = \frac{k_3 J'_{l;j}}{k_j J'_{l3}} a_{Elm;j} - \frac{k_j k_3}{k_2^2} \sqrt{l(l+1)} \bar{w}_{lm;j} \frac{J_{l;j}}{J'_{l3}} \quad (30p)$$

$$V_{2,Hlm}^{S_2} = \frac{\mu_3 H'_{l;j}}{\mu_2 J'_{l3}} a_{Hlm;j} \quad (30q)$$

$$V_{2,Elm}^{S_2} = \frac{k_3 H'_{l;j}}{k_j J'_{l3}} a_{Elm;j} - \frac{k_j k_3}{k_2^2} \sqrt{l(l+1)} \bar{w}_{lm;j} \frac{H_{l;j}}{J'_{l3}}. \quad (30r)$$

-
- [1] S. J. Oldenburg, R. D. Averitt, S. L. Westcott, and N. J. Halas, *Chem. Phys. Lett.* **288**, 243 (1998).
- [2] T. V. Teperik, V. V. Popov, and F. J. García de Abajo, *Phys. Rev. B* **69**, 155402 (2004).
- [3] E. Hao and G. C. Schatz, *J. Chem. Phys.* **120**, 357 (2004).
- [4] C. Tserkezis, G. Gantzounis, and N. Stefanou, *J. Phys.: Condens. Matter* **20**, 075232 (2008).
- [5] F. Le, D. W. Brandl, Y. A. Urzhumov, H. Wang, J. Kundu, N. J. Halas, J. Aizpurua and P. Nordlander, *ACS Nano* **2**, 707 (2008).
- [6] T. Christensen, A.-P. Jauho, M. Wubs, and N. A. Mortensen, *Phys. Rev. B* **91**, 125414 (2015).
- [7] N. T. Fofang, T.-H. Park, O. Neumann, N. A. Mirin, P. Nordlander, and N. J. Halas, *Nano Lett.* **8**, 3481 (2008).
- [8] J. A. Schuller, E. S. Barnard, W. Cai, Y. C. Jun, J. S. White, and M. L. Brongersma, *Nat. Mater.* **9**, 193 (2010).
- [9] C. Tserkezis, M. Wubs, and N. A. Mortensen, *ACS Photonics* **5**, 133 (2018).
- [10] F. Benz, M. K. Schmidt, A. Dreismann, R. Chikkaraddy, Y. Zhang, A. Demetriadou, C. Carnegie, H. Ohadi, B. D. Nijs, R. Esteban, J. Aizpurua, and J. J. Baumberg, *Science* **354**, 726 (2016).
- [11] J. B. Khurgin, *Nat. Nanotechnol.* **10**, 2 (2015).
- [12] D. G. Baranov, D. A. Zuev, S. I. Lepeshov, O. V. Kotov, A. E. Krasnok, A. B. Evlyukhin, and B. N. Chichkov, *Optica* **4**, 814 (2017).
- [13] A. B. Evlyukhin, S. M. Novikov, U. Zywiets, R. L. Erikssen, C. Reinhardt, S. I. Bozhevolnyi, and B. N. Chichkov, *Nano Lett.* **12**, 3749 (2012).
- [14] A. Garca-Etxarri, R. Gmez-Medina, L. S. Froufe-Prez, C. Lpez, L. Chantada, F. Scheffold, J. Aizpurua, M. Nieto-Vesperinas, and J. J. Senz, *Opt. Express* **19**, 4815 (2011).
- [15] F. Todisco, R. Malureanu, C. Wolff, P. A. D. Goncalves, A. S. Roberts, N. A. Mortensen, and C. Tserkezis, *Nanophotonics* **9**, 803 (2020).
- [16] P. Albella, M. A. Poyli, M. K. Schmidt, S. A. Maier, F.

- Moreno, J. J. Sáenz, and J. Aizpurua, *J. Phys. Chem. C* **117**, 13573 (2013).
- [17] E. Almpanis and N. Papanikolaou, *J. Opt. Soc. Am B* **33**, 99 (2016).
- [18] O. Yavas, M. Svedendahl, P. Dobosz, V. Sanz, and R. Quidant, *Nano Lett.* **17**, 4421 (2017).
- [19] S. Jahani and Z. Jacob, *Nature Nanotechnol.* **11**, 23 (2016).
- [20] I. Staude and J. Schilling, *Nat. Photonics* **11**, 274 (2017).
- [21] X. Zhu, W. Yan, U. Levy, N. A. Mortensen, and A. Kristensen, *Sci. Adv.* **3**, e1602487 (2017).
- [22] A. E. Krasnok, A. E. Miroshnichenko, P. A. Belov, and Y. S. Kivshar, *Opt. Express* **20**, 20599 (2012).
- [23] S. V. Li, D. G. Baranov, A. E. Krasnok, and P. A. Belov, *Appl. Phys. Lett.* **107**, 171101 (2015).
- [24] S. Raza, *Opt. Lett.* **45**, 1260 (2020).
- [25] T. K. Hakala, J. J. Toppari, A. Kuzyk, M. Pettersson, H. Tikkänen, H. Kunttu, and P. Trm, *Phys. Rev. Lett.* **103**, 053602 (2009).
- [26] C. Tserkezis, P. A. D. Gonalves, C. Wolff, F. Todisco, K. Busch, and N. A. Mortensen, *Phys. Rev. B* **98**, 155439 (2018).
- [27] H. Wang, Y. Ke, N. Xu, R. Zhan, Z. Zheng, J. Wen, J. Yan, P. Liu, J. Chen, J. She, Y. Zhang, F. Liu, H. Chen, and S. Deng, *Nano Lett.* **16**, 6886 (2016).
- [28] G. W. Castellanos, S. Murai, T. Raziman, S. Wang, M. Ramezani, A. G. Curto, and J. Gómez Rivas, *ACS Photonics* **7**, 1226 (2020).
- [29] R. Heilmann, A. I. Vkevinen, J.-P. Martikainen, and P. Trm, *Nanophotonics* **9**, 267 (2020).
- [30] K. Lodewijks, N. Maccaferri, T. Pakizeh, R. K. Dumas, I. Zubritskaya, J. kerman, P. Vavassori, and A. Dmitriev, *Nano Lett.* **14**, 7207 (2014).
- [31] D. K. Kim and J. Dobson, *J. Mat. Chem.* **19**, 6294 (2009).
- [32] Q. A. Pankhurst, J. Connolly, S. K. Jones, and J. Dobson, *J. Phys. D* **36**, R167 (2003).
- [33] S. P. Mornet, S. B. Vasseur, F. Grasset, and E. Duguet, *J. Mat. Chem.* **36**, 2161 (2004).
- [34] Z. Lin and S. T. Chui, *Phys. Rev. E* **69**, 056614 (2004).
- [35] P. Varytis and N. Stefanou, *J. Opt. Soc. Am. B* **33**, 1286 (2016).
- [36] P. Varytis and N. Stefanou, *Opt. Commun* **360**, 40 (2016).
- [37] V. Yannopapas and A. G. Vanakaras, *ACS Photonics* **2**, 1030 (2015).
- [38] V. Yannopapas, *Solid State Commun.* **217**, 47 (2015).
- [39] C. Wolff, R. RodriguezOliveros, and K. Busch, *Opt. Express* **21**, 12022 (2013).
- [40] L. D. Landau, E. M. Lifshitz, and L. P. Pitaevskii, *Electrodynamics of Continuous Media*, 2nd ed. (Butterworth-Heinemann, 1984).
- [41] A. Christofi and N. Stefanou, *Int. J. Mod. Phys. B* **28**, 1441012 (2013).
- [42] C. F. Bohren and D. R. Huffman, *Absorption and Scattering of Light by Small Particles* (Wiley, 1983).
- [43] J. D. Jackson, *Classical Electrodynamics*, 3d ed. (Wiley, 1999).
- [44] V. Doormann, J. P. Krumme, and H. Lenz, *J. Appl. Phys.* **68**, 3544 (1990).
- [45] T. Kim, S. Nasu, and M. Shima, *J. Nanoparticle Res.* **9**, 737 (2006).
- [46] P. Hansen, K. Witter, and W. Tolksdorf, *Phys. Rev. B* **27**, 6608 (1983).
- [47] P. Varytis, N. Stefanou, A. Christofi, and N. Papanikolaou, *J. Opt. Soc. Am. B* **32**, 1063 (2015).
- [48] P. Varytis, P. A. Pantazopoulos, and N. Stefanou, *Phys. Rev. B* **93**, 214423 (2016).
- [49] P. Trm and W. L. Barnes, *Rep. Prog. Phys.* **78**, 013901 (2014).
- [50] T. J. Antosiewicz, S. P. Apell, and T. Shegai, *ACS Photonics* **1**, 454 (2014).